

Tunable infrared generation in KTA and applications

G C BHAR*, P KUMBHAKAR, A K CHAUDHARY† and U CHATTERJEE

Laser Laboratory, Physics Department, Burdwan University, Burdwan 713 104, India

† Central Forensic Science Laboratory, 30-Gorachand Road, Calcutta 700 014, India

* Email: bdnvlib@giasl01.vsnl.net.in

MS received 12 April 1999

Abstract. Noncollinear difference frequency mixing of dye laser and Nd:YAG second harmonic (fundamental) radiation from a commercial laser system is employed for the generation of 2.7–5.3 μm (1.6–1.7 μm) radiations in a flux-grown KTiOAsO_4 crystal. The generated radiation is used to scan the methane absorption in the fundamental (ν_3) and its first overtone ($2\nu_3$) band at pressure 90 torr in a laboratory made single pass gas cell of length 33 cm.

Keywords. Nonlinear optics; frequency conversion; methane absorption.

PACS Nos 42.65.K; 86.70.L

1. Introduction

The infrared 2–5 μm region is rich in vibrational band of atmospheric gas molecules like CH_4 , CO , CO_2 , H_2CO , N_2O , SO_2 [1]. LiNbO_3 , LiIO_3 are used for the generation of 3–5 μm radiation. But the use of the LiIO_3 is disadvantageous as it is quite hygroscopic in nature and has a damage threshold of less than 150 MW/cm^2 . The damage threshold of LiNbO_3 is also rather low. Potassium Titanyl Phosphate (KTP) is an alternative crystal for the generation of mid-IR radiation [2], although the tunability in this crystal is limited to its transmission cut-off (4.5 μm). This crystal suffers gray tracking damage under intense laser radiation and good quality crystals devoid of gray tracking damage are yet to get wide acceptance. Another alternative biaxial crystal, Potassium Titanyl Arsenate (KTA), of KTP family is nonhygroscopic and its transmission cut-off is at 5.3 μm which is 1000 nm longer than that of KTP. The crystal KTA is also free of gray tracking damage and has slightly larger d_{eff} than that of KTP for some applications. Its laser damage threshold is an order of magnitude higher than that of LiIO_3 . Due to these advantageous characteristics KTA has attracted attention [3–5] for the generation of mid-IR radiation.

Methane is an important trace gas having significant effect in pollution of atmosphere. It has large number of absorption bands including a strong fundamental (ν_3) band and its first overtone ($2\nu_3$) band in the near infrared. By monitoring these absorption bands through laser probing it is possible to find the informations about its presence, concentration etc in the atmosphere. Using the systems reported earlier [6–9] it is possible to tune

only one band of methane. We generate tunable infrared radiations from 1.6–1.7 μm (and 2.7–5.3 μm) in a single set up by difference-frequency mixing of fundamental (second harmonic) of Nd:YAG radiation and dye laser radiation of a commercial laser system in the KTA crystal to scan both the overtone $2\nu_3$ as well as the fundamental ν_3 band of this important organic pollutant gas. The single pass gas cell of length 33 cm as well as methane gas used in the experiment is prepared in the laboratory. To the best of our knowledge for the first time we are reporting the simultaneous scan of ν_3 and $2\nu_3$ band, generating radiations in a single set up (allowed by the cut of the crystal for proper phase-matching) by difference frequency mixing of dye laser and Nd:YAG (its second harmonic) radiation in the KTA crystal. Optical parametric oscillation may be used instead of difference frequency mixing for the generation of IR radiation but difference frequency mixing is much simpler and has been proved by several researchers [6–8] that it is an effective scheme for the generation of stable narrow band tunable IR radiation. Also here the requirement of good beam quality and good quality crystals are not so important which are stringent factors in OPO. As another alternative source of infrared laser radiation in the wavelength range (1.5–3.0 μm) diode lasers are used based on semiconductor composition. But only a single laser has a very limited tuning range ($\sim 100 \text{ cm}^{-1}$) and power level in $\sim \mu\text{W}$. Moreover commercially available diode lasers do not cover continuously their nominal wavelength ranges and also require low temperature (100 K).

2. KTA absorption properties

The used KTA crystal is a flux-grown 7 mm cube and cut at $\varphi = 90^\circ$, $\theta = 36^\circ$ for phase-matching in the YZ -plane. The crystal is of water-white colour with a single striation multidomain that can be seen along the X -direction near the edge of one of two polished faces. We have used beams of diameters 4 mm and hence we got clear aperture for the input pump beams. Figure 1 shows the transmission characteristics of this KTA crystal and another 7 mm thick KTP crystal. The transmission of KTA extends down to 0.35 μm in the ultraviolet and up to 5.3 μm in the infrared i.e. 1000 nm further into the infrared than that of KTP and unlike KTP the O–H absorption band at 3–4 μm is absent in this crystal. The absorption coefficients a at different specific wavelengths have been calculated using the relation

$$a = -(1/l) \ln\left\{\frac{(B^2 + R^2)^{1/2} - B}{R^2}\right\}. \quad (1)$$

Here a is in cm^{-1} , length of the crystal l in cm, $B = (1 - R)^2/2T$ and $R = \{(n - 1)/(n + 1)\}^2$. T is the transmittance at different specific wavelength. The transmittance values at different wavelength have been measured by a Hitachi U-3400 (185–2600 nm) and an IR spectrophotometer Shimadzu (IR-470; 2.5–25 μm). In both the spectrophotometers light beams are unpolarised so for the calculation of the refractive index we used $n = (n_x + n_y + n_z)/3$ i.e. the average value of the principal refractive indices n_x , n_y and n_z along X , Y and Z direction, respectively. For the calculation of the principal refractive indices we have used the Sellmeier coefficients of Fennimore *et al* [3].

3. Experimental arrangements for difference frequency generation

The experimental arrangement is shown in figure 1 (inset). An electro-optically Q -switched Nd:YAG laser (Spectra Physics DCR-11, pulse width 10 ns and repetition rate

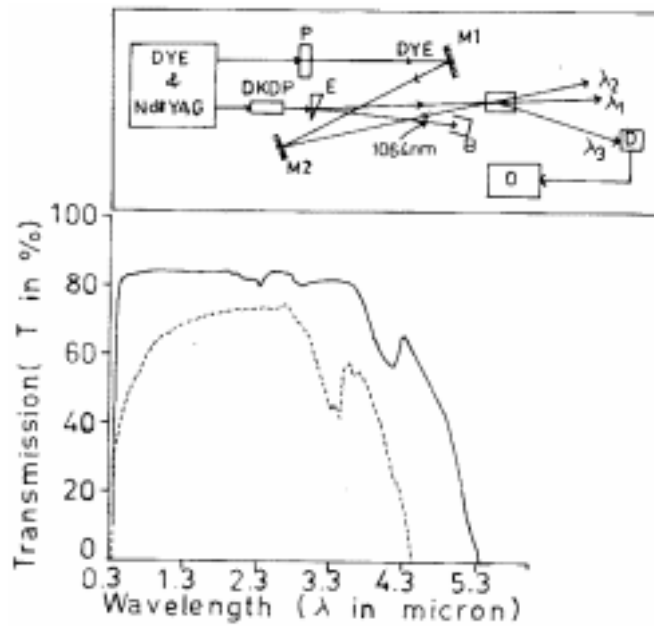


Figure 1. The solid curve illustrates the transmission (T in %) characteristics of KTA crystal used in the experiment and the dotted curve shows the same for KTP crystal. The schematic diagram of the experimental set-up is shown in the inset. M1, M2, mirrors; P, 90° polarization rotator for dye laser beam; B, 1064 nm beam dumper; E, extra dense flint glass prism meant for separation of 532 nm beam from 1064 nm beam; D, the liquid nitrogen cooled detector; O, oscilloscope.

10 Hz) and a dye laser (Spectra Physics PDL-2) pumped by the second harmonic of the same Nd:YAG laser have been used in the experiment. We used two dyes Rh-B and DCM to tune through the range 590–670 nm for the visible radiation for the generation of 1.6–1.7 μm and 2.7–5.3 μm radiation. To generate 2.7–5.3 μm radiation the residual pump beam (1064 nm) is again frequency doubled in a 3 cm long DKDP crystal to get 532 nm pump beam for DFM in KTA after its separation from the unconverted 1064 nm beam through an extra dense flint (EDF) glass prism. The polarization state of dye beam being vertical, we pass it through a 90° polarization rotator to get appropriate polarization states of the input beams for type-II (i.e. $o - e \rightarrow o$) DFM in the KTA crystal while we rotate the crystal KTA in the horizontal (YZ) plane. For the generation of 1.6–1.7 μm radiation we do not require to use the DKDP crystal the pump beam being 1064 nm itself. For type-II DFM the required polarization of input 1064 nm and dye laser beams are extraordinary and ordinary and that of the generated beam is ordinary i.e. $o - e \rightarrow o$ interaction have been used. To avoid the use of filters for the separation of generated beam (1.6–1.7 μm and 2.7–5.3 μm) from the input parent beams we use non-collinear frequency mixing scheme and an external angle of $\sim 2.3^\circ$ (which corresponds to an internal angle $\sim 1.3^\circ$) between the input beams sufficiently separates the generated radiations from its parent beams within a distance of only 15 cm from the exit face of the crystal. The generated infrared radiation

has been detected by a liquid nitrogen cooled HgCdTe detector. We run the transmission/absorption characteristics of a standard polystyrene sheet supplied by M/s Shimadzu Corporation for the calibration of the generated radiation.

4. Phase-matching characteristics for DFG

The phase-matching angle (θ) have been calculated by solving numerically the following equations, obtained from the conservation of momentum and energy in the three-wave interaction under consideration when the internal noncollinear angle between the two input parent beams is 1.3° . Equations are

$$\vec{K}_1^X - \vec{K}_2^{YZ} = \vec{K}_3^X \quad (2a)$$

and

$$1/\lambda_1 - 1/\lambda_2 = 1/\lambda_3. \quad (2b)$$

Here, \vec{K}_1^X , \vec{K}_2^{YZ} and \vec{K}_3^X are wavevectors for λ_1 , λ_2 and λ_3 beams, respectively. Figure 2 shows the phase-matching characteristics for the generation of 2.7–5.3 μm radiation by type-II ($o - e \rightarrow o$) DFM of dye laser radiation (λ_2) and 532 nm (λ_1) radiation. Phase-matching occurs in the YZ -plane of the crystal. In this case the light polarized along the X -direction behaves as vertically polarized ordinary wave and that polarized in the YZ -plane behaves as horizontally polarized extraordinary wave. Calculated phase-matching

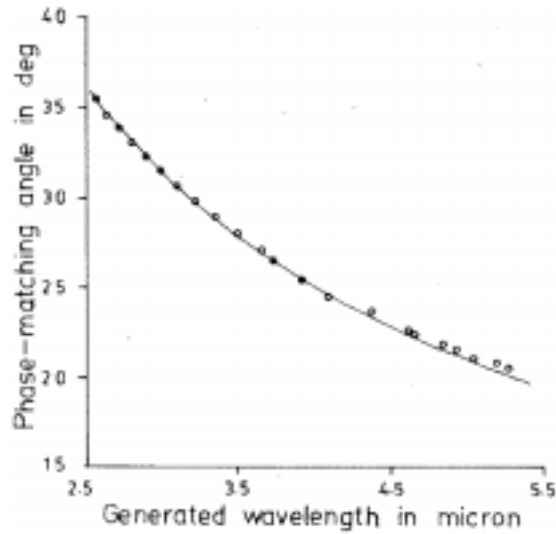


Figure 2. Illustration of angular phase-matching characteristics for generation of 2.7–5.3 μm radiation in the crystal KTA by DFM when the noncollinear angle between the input parent beam is 1.3° . Solid curve is the theoretical prediction as obtained using Sellmeier coefficients of Fennimore *et al* [3] and small circles are experimental points.

(internal) angles are polar angles made by the generated beam with the Z -axis obtained from the measured external angles [10]. The measured value of the external angular bandwidth and the phase-matched spectral bandwidth for generation of $3.48 \mu\text{m}$ by DFM of 532 nm and 628 nm beams for internal noncollinear angle $\sim 1.3^\circ$ is 1.9 mrad and 14 nm-cm which agrees reasonably well to the calculated value of 1.6 mrad and 13.9 nm-cm, respectively.

For the generation of 1.6–1.7 μm radiation dye laser (639–655 nm) and 1064 nm (Nd:YAG) radiations have been used as λ_1 and λ_2 beam, respectively. In this case also the type-II ($o - e \rightarrow o$) interaction have been used in the $Y Z$ -plane of the same KTA crystal with the same noncollinear angle (1.3°) between the input beams. The phase-matching angle varies from 44° to 47° for the generation of 1.6 μm to 1.7 μm .

5. DFG power

Some preliminary measurement of the energy of the generated radiation (2.7–5.3 μm) have been done without giving any attention to the efficiency of the process. The solid curve in figure 3 shows the variation of the power of the generated radiations with the generated wavelength while the 532 nm beam energy is kept fixed at 10 mJ (which corresponds to a power density of 800 KW/cm^2) and dots are experimental points. As we have used unfocussed beam, diffraction spreading of the beam are neglected. Assuming plane-wave theory and since the conversion efficiency is quite less than 10%, we used the following

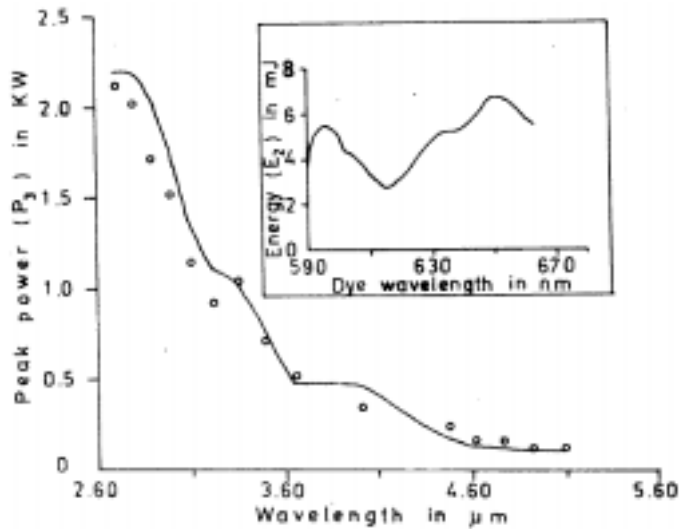


Figure 3. Variation of the power of the generated infrared radiation (P_3) at different generated wavelengths due to the variation of the input dye laser energy keeping the 532 nm beam energy fixed at 10 mJ (which corresponds to the peak power density of 800 KW/cm^2). Circles are experimental points and the solid curve is the theoretical prediction. Inset shows the variation of the input dye laser energy (E_2) with its wavelength (λ_2).

expression for theoretical calculation [11]

$$P_3 = P_1 P_2 \{ (52.2 l^2 d_{\text{eff}}^2 T_1 T_2 T_3 F) / (n_1^0 n_2^e(\theta) n_3^0 \lambda_3^2 A) \}, \quad (3)$$

where P_i 's are powers for λ_i 's beams. l is the crystal length in cm and θ is the phase-matching angle, n_1^0 , $n_2^e(\theta)$ and n_3^0 are refractive indices for λ_1 (532 nm), λ_2 (dye), and λ_3 beam, respectively. T_i 's are first surface transmission for λ_i 's beams and A is the area of cross section of the interacting beams. F is the absorption factor calculated from the relation

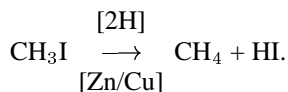
$$F = \{ (1 - 2e^{-a'/2} + e^{-a'}) / (a'/2)^2 \} e^{-a_3 l} \quad (4)$$

where, $a' = (a_1 + a_2 - a_3)l$. a_1, a_2, a_3 are the absorption coefficients in cm^{-1} of the crystal at the three wavelengths λ_1, λ_2 and λ_3 , that have been obtained from eq. (1).

We have not done any detail energy measurement for 1.6–1.7 μm as the aim was to scan the two band (ν_3 and $2\nu_3$) of methane by generating radiation in an almost same and also simple set up. In the process a minimum power of 100 W have been obtained throughout the total tuning range 1.6–1.7 μm and 2.7–5.3 μm which is quite sufficient for the probe type experiment.

6. Absorption spectra of methane

The single pass gas cell of length 33 cm is designed indigenously in the laboratory. It is made of borosil glass which has two calcium fluoride windows each of diameter 2.5 cm. Windows are kept in holders using neoprene O-rings. The cell has three stopcocks, out of which one is used to connect a vacuum pump and another one is connected to the gas jar. The third one is connected with a pressure gauge which constantly measures the pressure of the gas within the cell. Time to time cleaning of the cell is required and our design provides that facility. The methane used in the experiment is also prepared in the laboratory. It is produced by the reduction of methyl iodide by nascent hydrogen and then purified. Nascent hydrogen is produced by the chemical reaction of methyl alcohol with zinc–copper couple. This nascent hydrogen reduces methyl iodide to produce methane gas mixed with residual methyl iodide and hydrogen iodide.



The gas mixture is passed through a U-tube placed on freezing-mixture where methyl iodide is trapped as it liquifies and the gaseous methane is filled in a gas jar by the displacement of water. Then the gas is passed through concentrated H_2SO_4 and thereafter the pure gas is collected by the displacement of mercury. Using a needle-valve arrangement we then fill the gas cell with methane at a pressure of 90 torr for studying its absorption characteristic. Before filling the cell with methane, we evacuate it using a rotary vacuum pump. Transmission at each wavelength is calculated by taking the ratio of the transmitted pulse energy through the cell to the incident energy. We scan the $2\nu_3$ band and P -branch of the ν_3 band of the methane absorption spectrum by varying the dye laser wavelength using its in-built grating tuning arrangement of the dye laser system and with

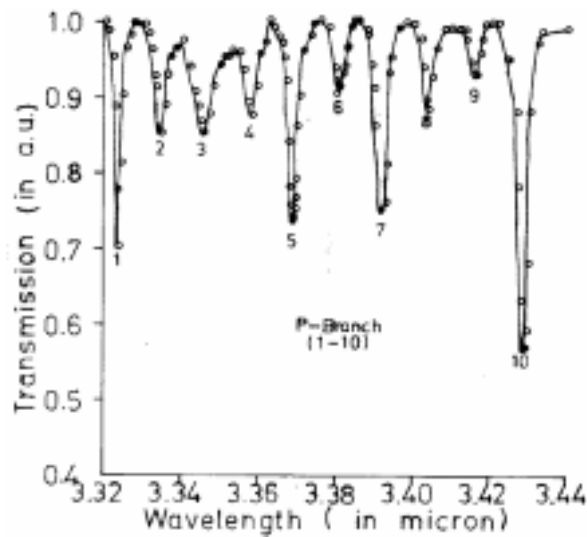


Figure 4a. Transmission characteristics of methane at 90 torr pressure in the P -branch of the fundamental (ν_3) band. Circles are experimental points and the solid curve is drawn only to show the trends of the datas. The numbers 1–10 have been explained in table 1.

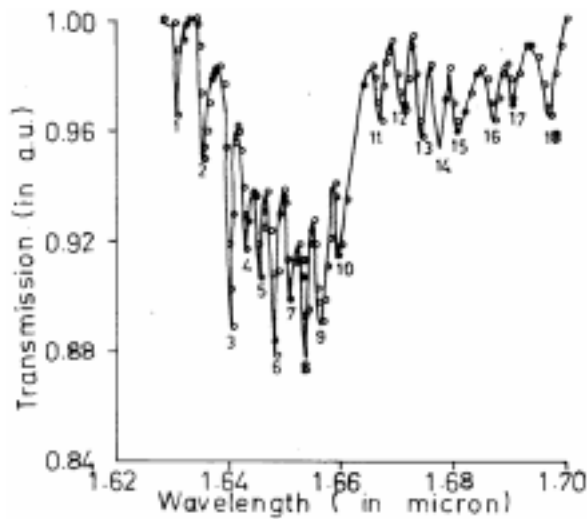


Figure 4b. Transmission characteristics of methane at 90 torr pressure in the overtone ($2\nu_3$) band. Circles are experimental points and the solid curve is drawn only to show the trends of the datas. The numbers 1–18 have been explained in table 2.

the proper rotation of the crystal. The spectral phase-matched bandwidth of the crystal for the generation of $3.48 \mu\text{m}$ has been measured and it is $\sim 14 \text{ nm-cm}$. Therefore we require to tune the crystal after complete scanning of a single line by tuning

the dye laser wavelengths only and this saves the time and increases the ease of work. The transmission from the gas cell at each wavelength has been normalized by taking a transmission measurement with no methane in the cell. The transmission characteristics (with 1% transmission resolution) as we obtain are shown in figures 4a and 4b. From these figures it is clearly seen that the ν_3 band is stronger than $2\nu_3$ band of methane. For the measurement of intensity of the transmitted signal beam we use calibrated LN_2 cooled HgCdTe detector with the responsivity 40 V/W. The signal to noise ratio

Table 1. Observed P -branch of ν_3 band of methane.

| Nos shown in figure 4a | Wavelength (μm) | Assignments (values within the bracket are the J^* values) |
|------------------------|------------------------------|--|
| 1 | 3.3234 | $P(1)$ |
| 2 | 3.3345 | $P(2)$ |
| 3 | 3.3456 | $P(3)$ |
| 4 | 3.3570 | $P(4)$ |
| 5 | 3.3687 | $P(5)$ |
| 6 | 3.3806 | $P(6)$ |
| 7 | 3.3916 | $P(7)$ |
| 8 | 3.4037 | $P(8)$ |
| 9 | 3.4165 | $P(9)$ |
| 10 | 3.4283 | $P(10)$ |

*Rotational quantum number.

Table 2. Observed $2\nu_3$ band of methane.

| Nos shown in figure 4b | Wavelength (μm) | Assignments (values within the bracket are the J^* values) |
|------------------------|------------------------------|--|
| 1 | 1.6305 | $R(12)$ |
| 2 | 1.6354 | $R(10)$ |
| 3 | 1.6404 | $R(8)$ |
| 4 | 1.6429 | $R(7)$ |
| 5 | 1.6455 | $R(6)$ |
| 6 | 1.6482 | $R(5)$ |
| 7 | 1.6509 | $R(4)$ |
| 8 | 1.6537 | $R(3)$ |
| 9 | 1.6565 | $R(2)$ |
| 10 | 1.6594 | $R(0)$ |
| 11 | 1.6671 | $Q(10)$ |
| 12 | 1.6714 | $P(2)$ |
| 13 | 1.6764 | $P(3)$ |
| 14 | 1.6776 | $P(4)$ |
| 15 | 1.6808 | $P(5)$ |
| 16 | 1.6873 | $P(7)$ |
| 17 | 1.6906 | $P(8)$ |
| 18 | 1.6973 | $P(10)$ |

*Rotational quantum number.

of the detector is greater than 20. The assignment of the lines numbered 1–10 in figure 4a and 1–18 in figure 4b are shown separately in tables 1 and 2, respectively. We were able to identify all the lines of P branch of ν_3 band. However with the available resolution of our system some of the lines of P, Q, R branches of $2\nu_3$ band can only be identified. Moreover, the weak absorption of methane in this region may also limit our measurement.

The absorption coefficients values (α_{CH_4}) for $P(5)$ lines of ν_3 band of methane as obtained using Beer–Lambert law have been plotted with the wave number (cm^{-1}) as shown in the figure 5. The Beer–Lambert law is given by

$$\alpha_{\text{CH}_4} = (1/pL) \ln(T'/T_0')$$

where, p is the methane gas pressure (90 torr, in our case), L is the cell length (33 cm, in our case). T' and T_0' are transmissions with and without gas in the cell. The solid curve of figure 5 has been fitted assuming Lorentzian line-profile and $\Delta\nu$ equals to 1 cm^{-1} . The Lorentzian function is given by

$$\alpha_{\text{CH}_4}(\nu)/\alpha_{\text{CH}_4} = \Delta\nu^2 / \{(\nu - \nu_0)^2 + \Delta\nu^2\},$$

where $\alpha_{\text{CH}_4}(\nu)$ and α_{CH_4} are the absorption coefficients at the frequency ν (cm^{-1}) and at the centre frequency (ν_0 , in cm^{-1}).

The spectral resolution of the generated infrared radiation is seen to be better than 1 cm^{-1} (HWHM) as obtained by fitting the Lorentzian line-profile for the measured spectrum of $P(5)$ line of ν_3 band of methane.

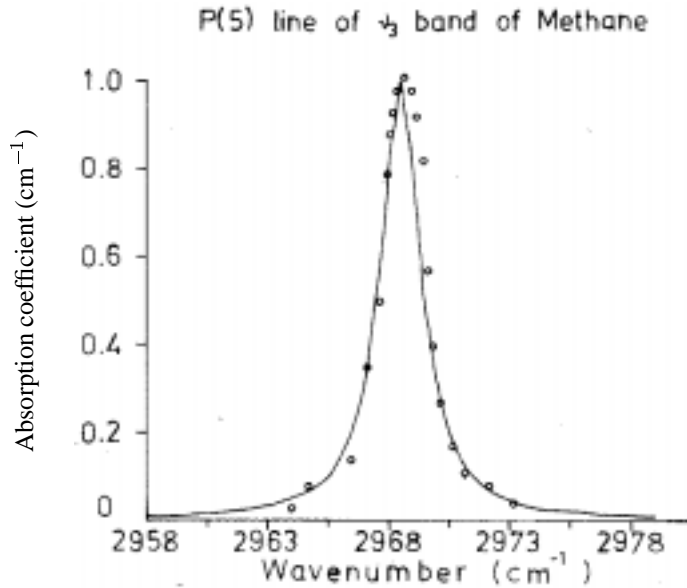


Figure 5. Absorption coefficient (α_{CH_4}) values (in a.u.) for $P(5)$ line of ν_3 band of methane have been plotted with the wave numbers (cm^{-1}). Solid curve is the fitted spectrum assuming Lorentzian line-shape and $\Delta\nu = 1 \text{ cm}^{-1}$. Small circles are experimental points obtained from Beer–Lambert law.

7. Conclusions

Using an indigenously made single pass 33 cm long gas cell we were able to scan both the fundamental (ν_3) and the first overtone ($2\nu_3$) band of methane by generating tunable radiation 1.6–1.7 μm (2.7–5.3 μm) using difference-frequency mixing of a dye laser and Nd:YAG (its second harmonic) in a single KTA crystal. The spectral resolution of the generated infrared radiations have also been measured which is better than 1 cm^{-1} (HWHM). In the process of DFG we obtained $>100\text{ W}$ of peak power for the full tuning range. Further work will be done for narrowing the line-width of the laser by using etalon in the dye laser cavity to find the finer details of the lines for more spectroscopic informations and also to increase the conversion efficiency of the process thereby increasing the generated energy.

Acknowledgements

Authors acknowledge the National Laser Programme, Govt. of India, for the partial financial support and one of the authors (PK) is thankful to UGC for his maintenance fellowship. The authors are also grateful to Dr A K Mukherjee of Chemistry Department, and Shri A Ghosh of Basic and Synthetic and Chemical Pvt. Ltd., Jadavpur, Calcutta, for assistance in the experiment.

References

- [1] L S Rothman, R R Gamache, A Goldman, L R Brown, R A Toth, H M Pickett, R L Poynter, J M Flaud, C Camypeyret, A Barbe, N Husson, C P Rinsland and M A H Smith, *Appl. Opt.* **26**, 4058 (1987)
- [2] G C Bhar, U Chatterjee, A M Rudra and A K Chaudhary, *J. Phys.* **D30**, 2693 (1997)
- [3] D L Fennimore, K L Schepler, U B Ramabadran and S R Mcpherson, *J. Opt. Soc. Am.* **B12**, 794 (1995)
- [4] A H Kung, *Appl. Phys. Lett.* **65**, 1082 (1994)
- [5] K Kato, N Umemura and E Tanaka, *Jpn. J. Appl. Phys.* **36**, L403 (1997)
- [6] D G Lancaster and J M Dawes, *Opt. Commun.* **120**, 307 (1995)
- [7] K P Petrov, S Waltman, U Simon, R F Curl, F K Titel, E J Dlugokencky and L Hollberg, *Appl. Phys.* **B61**, 553 (1995)
- [8] L Goldberg, J Koplow, D G Lancaster, R F Curl, and F K Titel, *Opt. Letts.* **23** 1517 (1998)
- [9] K Uehara and H Tai, *Appl. Opt.* **31**, 809 (1992)
- [10] G C Bhar and U Chatterjee, *Jpn. J. Appl. Phys.* **29**, 1103 (1990)
- [11] F Zernike, *Methods of experimental physics*, part B, edited by C L Tang (Academic Press, New York, 1979) vol. 15, pp 143–183